Binary Local Fractal Dimension: a Precise Structure Parameter for 3D High Resolution Computed Tomography Images of the Human Spongiosa

Felix Thomsen[1], Jaime Peña[2], Jan Bastgen[2], Beata Hoffmann[3], Isolde Frieling[4], Claus-C. Glüer[2], and Claudio Delrieux[1]

[1] Imaging Sciences Lab, Universidad Nacional del Sur, Bahía Blanca, Argentina, FelixThomsen@yahoo.de
[2] Biomedical Imaging, Klinik für Diagnostische Radiologie, Christian-Albrechts-Universität zu Kiel, Germany
[3] Diagnostische Radiologie, Klinik für Diagnostische Radiologie, Christian-Albrechts-Universität zu Kiel, Germany
[4] Osteoporosezentrum Hamburg - Neuer Wall, Hamburg, Germany

Abstract. We present the Binary Local Fractal Dimension (LFD) to analyze osteoporosis induced fracture risk with clinical 3D high resolution quantitative computed tomographic (HRCT) images of human vertebrae. We test if LFD parameters provide precise additional information besides bone mineral density (BMD) and standard descriptors of bone quality, for example bone surface ratio (BS/BV). We define a weighted LFD (wLFD) using the $\bar{R}^2$ of the Hölder exponents. We compare the LFD with standard methods (distance transform, direct secant method and run-length method) on 5 vertebrae $\times$ 8 volumes of interest and 5 repeated scans. The wLFD contains the highest direct and BMD-independent precision ($R^2 = 0.985$ and $R^2 = 0.949$), followed by BS/BV ($R^2 = 0.977$ and $R^2 = 0.920$) including low correlation with BMD (wLFD: $R^2 = 0.704$, BS/BV: $R^2 = 0.814$). LFD improves the translation from reference μCT- to clinical HRCT-resolution. In conclusion, LFD provides a strong diagnostic tool to characterize bone quality to predict osteoporosis induced fracture risk.

Keywords: Binary local fractal dimension, Hölder exponent, HRCT, qualitative structure parameter

1 Introduction

Osteoporosis is a skeletal disorder characterized by weak bone strength and high fracture risk. Bone strength reflects primary bone mineral density (BMD) and bone quality, which means architecture, turnover, damage accumulation, and mineralization [2]. The bone quality can be measured by parameters such as the trabecular separation (Tb.Sp), trabecular thickness (Tb.Th), trabecular number (Tb.N), bone surface by bone volume (BS/BV), bone volume by total volume

(BV/TV), and the mean intercept length of the bone phase and its 3-dimensional distribution, which can be described by the 3 eigenvalues and the derived degree of anisotropy (DA)[3].

The qualitative parameters have been originally defined for 2D-histomorphometry or ex-vivo micro quantitative computed tomography μCT, but have been also accepted on clinical HRQCT with much lower resolution at present pharmaceutical studies (see [7] and [5]). At clinical HRCT resolution, the qualitative parameters are also called apparent measures as partial volume effect, blurring and noise affect the assessment [13], see Fig. 1. In this paper, we will nevertheless avoid this nomenclature.

The local fractal dimension (LFD) or distribution of Hölder exponents α analyzes the local intrinsic dimension of a binary surface. This technique has been used for image segmentation [16] and extensively as a first step of multifractal analyses ([12] and references therein). We apply the method as a pure structure parameter of bone. We analyze in this paper a version of the LFD, which uses the same binary segmentation as the standard qualitative parameters. We aim to demonstrate that the LFD can be used as a precise qualitative bone structure parameter and that the information derived with the LFD is highly orthogonal to the one of the BMD, meaning that it provides BMD-independent information about the bone quality. Further, we suggest that the distinction of different degrees of osteoporosis can be noticeably enhanced by including the LFD in the toolbox of established HRCT parameters.

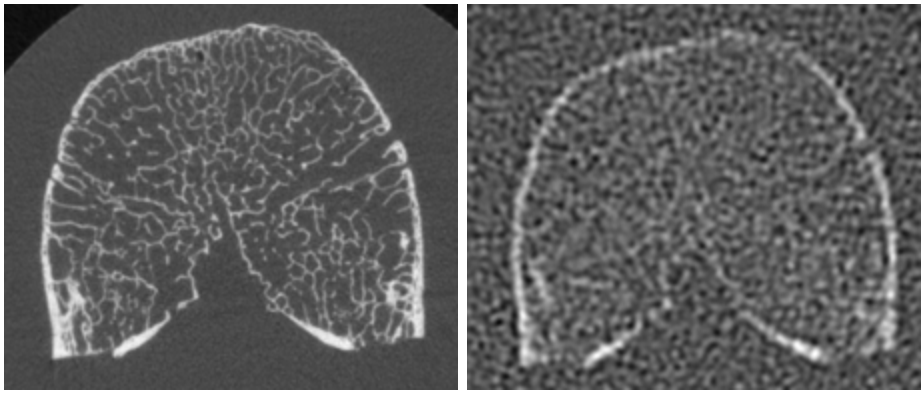

Fig. 1. Gold standard μCT (left) resolves the trabecular network nearly optimal. In-situ HRCT (right) includes noise, blurring and low resolution yielding apparent measures.

2 Materials and methods

2.1 Scans

We manufactured 5 vertebra phantoms by embedding vertebral bodies (T12 and L1) in epoxy resin (Technovit Epox, Heraeus Kulzer GmbH, Hanau, Germany). The vertebrae were obtained from the anatomical institute of the Christian-Albrechts-University at Kiel, Germany and the department of legal medicine of the University Hospital Hamburg-Eppendorf, Germany. The vertebra phantoms were inserted in an abdomen phantom (Model 235, Computerized Imaging Reference Systems Inc, Norfolk, VA, USA) and scanned with a clinical CT-scanner (Somatom Sensation 64, Siemens AG, Forchheim, Germany) using a HRCT protocol ($120kV$, $355mAs$, voxel size $188 \times 188 \times 300\mu m^3$, slice thickness $600\mu m$).

We repeated the measurements 3 times and again 2 times by using an additional body ring, see Fig. 2. The 3 repeated scans are useful to analyze the impact of noise, whereas the other 2 scans simulate obese patients. Taking the 5 scans together, we are able to test the robustness of the analyses against changes in patient size. HRCT data were calibrated to mineral scale [mg K_2HPO_4/cm^3] using a calibration phantom (Model 3 CT Calibration Phantom, Mindways Software, Austin, TX, USA) and the software Structural Insight (Structural Insight 3.1, Biomedical Imaging, University of Kiel, Germany).

For each vertebra phantom we obtained one gold standard μCT reference measurement (XCT, Scanco Medical AG, Bassersdorf, Switzerland, $59.4kV$, $74.8mAs$, voxel size $82 \times 82 \times 82\mu m^3$) without abdomen phantom, Fig. 2. We scanned the vertebra phantom without abdomen phantom and calibrated the data to mineral scale [mg $CaHA/cm^3$] with the automatic procedure of the μCT-device.

2.2 Image Processing

We defined on each of the 5 μCT images 8 disjoint volumes of interest inside the spongiosa (size: $800mm^3 - 975mm^3$ depending on the vertebra) and we registered the volumes of interest to all corresponding HRCT scans, using Structural Insight. The registration automatically rotated and translated the volumes of interest without altering the actual image data.

The comparison between repeated scans was achieved on the structure parameters derived from related volumes of interest but not from related voxels. For the qualitative structure parameters we binarized the images with a global threshold of 250 mg K_2HPO_4/cm^3 or respectively 250 mg $CaHA/cm^3$.

2.3 Standard Structure Parameters

We implemented a representative set of standard structure parameters which were already used in present pharmaceutical studies (e.g. [7] and [5]). We considered BMD and BV/TV, structure parameters based on the distance transform

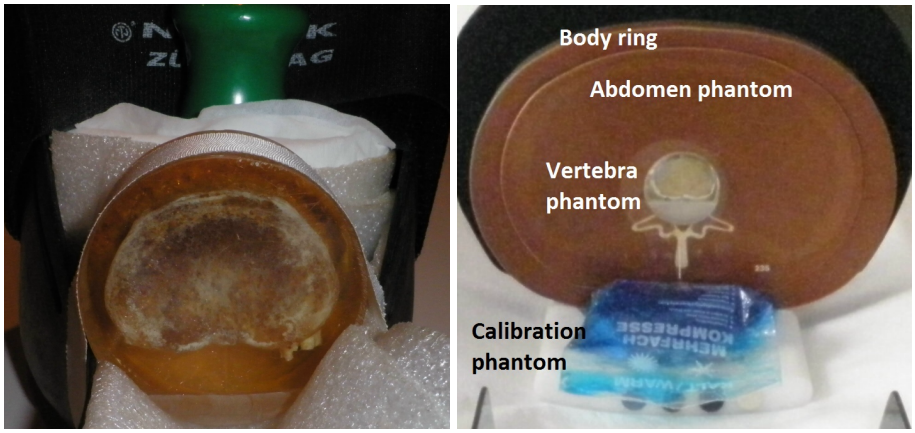

Fig. 2. μCT setup (left): The vertebra phantom is scanned without abdomen phantom (ex situ). HRCT setup (right): The vertebra phantom is embedded in the abdomen phantom with body ring (in situ). The calibration phantom enables to achieve accurate density values.

(DT) [9], on the direct secant method (DSM) [18] and [8], and the run-length method (RLM) [3] and [8].

In the applied version of Structural Insight the DSM and RLM was not only able to analyze ellipsoidal volumes, as proposed in [17], but treated all shapes accordingly. The histograms of the run-lengths of the bone- and marrow-phase were evaluated by the median, giving the $\mathrm{Tb.Th_{RLM}}$ and $\mathrm{Tb.Sp_{RLM}}$.

The parameters of the DSM were derived from Tb.N and BV/TV using the parallel plate model [17] with

$$\mathrm{Tb.Sp_{DSM}} = (1 - \mathrm{BV/TV})/(\mathrm{Tb.N}),$$

$$\mathrm{Tb.Th_{DSM}} = (\mathrm{BV/TV})/(\mathrm{Tb.N}), \text{and}$$

$$\mathrm{BS/BV} = (\mathrm{Tb.N})/(\mathrm{BV/TV}).$$

The degree of anisotropy was $\mathrm{DA} = 1 - \mathrm{eigenvalue_3/eigenvalue_1}$, the eigenvalues represent the lengths of the main axes of the ellipsoid derived from the 3D-distribution of the mean intercept lengths [19] with $\mathrm{eigenvalue_1}$ the largest and $\mathrm{eigenvalue_3}$ the smallest eigenvalue. Due to poor performance on HRCT we applied the DA only on the μCT reference measurements.

2.4 The Binary Local Fractal Dimension

The binary local fractal dimension (LFD) uses the same binarization and the same regions of interest as the standard qualitative structure parameters. We define the LFD as the distribution of all local Hölder exponents α inside the segmented regions (bone or marrow).

First we create a map between Euclidean radii and pseudo radii using positions in a $1mm$ neighborhood with the given grid-spacing:

$$\text{Volume}_{\text{Max}}(r) = |\{p_i : \text{Distance}_{\text{Euclid}}(0, p_i) \leq r\}|$$

with $\text{Distance}_{\text{Euclid}}(p_1, p_2)$ the euclidean distance (in mm) between p_0 and p_1, and

$$r_{\text{pseudo}}(r) = \sqrt[3]{\text{Volume}_{\text{Max}}(r)}.$$

Assume we want to calculate the α at a given position p which belongs to $\text{phase}_1 \in \{\text{bone}, \text{marrow}\}$, where bone depicts the bone phase generated by the binarization and marrow is the dual bone phase. We count all voxels p_i belonging to $\text{phase}_2 \in \{\text{bone}, \text{marrow}\}$ as the integral of a function of the distance to p:

$$\text{Volume}(r) = |\{p_i : \text{Distance}_{\text{Euclid}}(p, p_i) \leq r \wedge \text{Phase}(p_i) = \text{phase}_2\}|$$

with $\text{Phase}(p_i)$ returning the phase at position p_i. Finally we create an $x-$ and an $y-$vector with $x = \log(r_{\text{pseudo}})$ and $y = \log(\text{Volume})$. We calculate the slope of the linear fit between the first n entries of x and y, where n maximizes the adjusted coefficient of determination which is in the our case: $\bar{R}^2 = R^2 - (1 - R^2)/(n - 2)$.

The slope of the linear fit equals the local α and the LFD-distribution is defined as the density function of these local α's. We define a weighted LFD-distribution similar to the non-weighted LFD-distribution, but with the only difference that each α integrates in the density function wLFD with its individual weight depending on $\bar{R}^2$ as follows: w= $(\bar{R}^2)^{1000}$. With this weighting function we exclude practically all α's with too low $\bar{R}^2$ and enhance these with $\bar{R}^2$ near 1, which implies that poorly estimated local dimensions are partially excluded from the distribution, see Fig. 3.

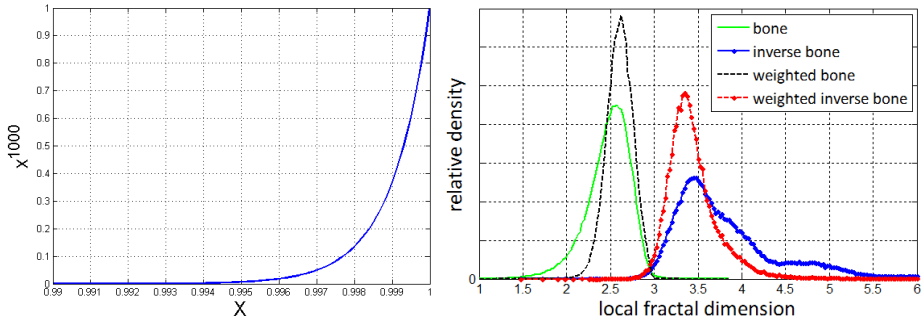

Fig. 3. Left: The weighting function practically excludes all α's with insufficient high $\bar{R}^2$ (=X). Right: The four LFD-Bone-distributions of an example HRCT-scan. The weighted LFD's (black and red) contain lower standard deviations than the not weighted LFD's (green and blue).

By combining the two phases: phase_1 and phase_2 and including the weighting function, we are able to generate 8 different distributions from that we can derive the average and the standard deviation, hence we have 16 structural parameters. With preliminary analyses we shrinked the set of possible LFD-parameters to the 6 most precise ones:

$\mathbf{LFD}_{\text{Bone}}$ is the average of the distribution, generated by $\text{phase}_1 = \text{phase}_2 =$ bone, $\mathbf{wLFD}_{\text{Bone}}$ is the average of the weighted distribution: $\text{phase}_1 = \text{phase}_2 =$ bone. $\mathbf{LFD}_{\text{InverseBone}}$ is the average of $\text{phase}_1 =$ marrow and $\text{phase}_2 =$ bone. $\mathbf{LFD\_SD}_{\text{Marrow}}$ denotes the standard deviation with $\text{phase}_1 = \text{phase}_2 =$ marrow and $\mathbf{wLFD\_SD}_{\text{Marrow}}$ its weighted pendant. $\mathbf{LFD\_SD}_{\text{InverseBone}}$ stands for the standard deviation of the distribution with $\text{phase}_1 =$ marrow and $\text{phase}_2 =$ bone.

2.5 Evaluation

We derive BMD-independent information of each structure parameter (sp) as a shifted residual of the linear fit of sp with the BMD: $sp(\widehat{\text{BMD}}) = a + b\text{BMD}$ and $sp_{\text{BMDindependent}} = sp - b\text{BMD}$. This is the additional explicatory power of the structure parameter after including the BMD in a linear discriminant analysis.

We apply ANOVA-tests to achieve the precision of each structure parameter, since it is a generalization of the t-test for more than 2 groups. The R^2 of the ANOVA is defined as

$$R^2 = \frac{\text{Sum Squares(Model)}}{\text{Sum Squares(Total)}} = \frac{\sum (sp_{i,j} - \overline{sp})^2 - \sum (sp_{i,j} - \overline{sp_j})^2}{\sum (sp_{i,j} - \overline{sp})^2},$$

with $sp_{i,j}$ the structure parameter of scan i and region j, $\overline{sp}$ the average structure parameter of the complete population and $\overline{sp_j}$ the average structure parameter of the given region j. We take the 3 or 5 repeated measurements (scans) and the 5 vertebra phantoms $\times$ 8 volumes of interest (regions).

We achieve the accuracy of the HRCT-parameters for predicting the BMD-orthogonal information of the μCT-parameters by multivariate regressions between the μCT and HRCT-parameters. The evaluation of the structure parameters was performed with a statistics program (JMP 7.0, SAS Institute, Cary, NC, USA).

3 Results

ANOVA tests of the direct structure parameters with 3 repeated scans show highest precision for the $\text{wLFD}_{\text{Bone}}$ ($R^2 = 0.98$). The BMD (3 scans: $R^2 = 0.97$) and the Tb.Th (DSM: $R^2 = 0.97$, DT: $R^2 = 0.97$) reached similar high precisions - but also the LFD_{Bone} ($R^2 = 0.97$) and the $\text{LFD\_SD}_{\text{InverseBone}}$ ($R^2 = 0.97$), see Fig. 4. By including the 2 scans with body ring the BMD became the most precise parameter ($R^2 = 0.97$), the $\text{wLFD}_{\text{Bone}}$ ($R^2 = 0.95$) became the second most precise parameter (not shown).

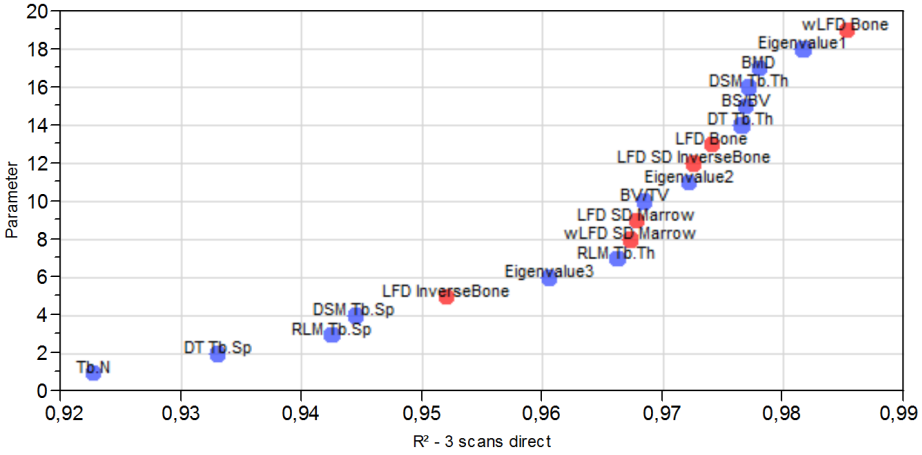

Fig. 4. R^2 of the structure parameters with 3 repeated scans without body rings, the y-axis contains the parameter while the x-axis contains the R^2. Red symbols depict the LFD-parameters, the standard parameters are blue. The $\text{wLFD}_{\text{Bone}}$ is most precise followed by the 1. eigenvalue, the BMD, $\text{Tb.Th}_{\text{DSM}}$ and BS/BV.

The direct structure parameters were often strongly correlated with the BMD and the measured precision was therefore induced by that correlation. The highest correlations with the BMD were obtained by BV/TV ($R^2 = 0.96$) and Tb.Sp (DSM: $R^2 = 0.94$, RLM: $R^2 = 0.94$). The $\text{LFD}_{\text{InverseBone}}$ and the $\text{wLFD}_{\text{Bone}}$ least correlated with the BMD ($R^2 = 0.66$ and $R^2 = 0.70$), followed by the Tb.Th_{DT} ($R^2 = 0.71$) and BS/BV ($R^2 = 0.81$), see Fig. 5.

The precision of the BMD-independent information of the structure parameters was derived with ANOVA-tests. The values can be interpreted as the precision of the structure parameters without any bias of the BMD. The most precise BMD-independent information was generated by the $\text{wLFD}_{\text{Bone}}$ (3 scans: $R^2 = 0.94$, 5 scans: $R^2 = 0.84$). The BS/BV showed high precision for the setting with 3 scans ($R^2 = 0.92$) but much lower precision for the setting with 5 scans ($R^2 = 0.69$). The $\text{LFD\_SD}_{\text{InverseBone}}$ ($R^2 = 0.76$) showed the second best correlation for the setting with 5 scans, see Fig. 6. The $\text{wLFD}_{\text{Bone}}$ showed the most robust performance against the interference induced by the artificial heterogeneous patient's body mass simulated by including the 2 scans with body ring.

The accuracy of the BMD-independent measurements was derived by correlations between all μCT- and HRCT-parameters. For each μCT-parameter, the HRCT standard parameter with the highest correlation to the μCT-data was compared with the LFD-parameter with the highest correlation to the μCT-data. The approximations improved nearly always by switching to the LFD parameters. The $\text{wLFD}_{\text{Bone}}$ approximated μCT's Tb.Sp (DSM: $R^2 = -0.711$, RLM: $R^2 = -0.718$, DT: $R^2 = -0.418$) and showed also good results for the

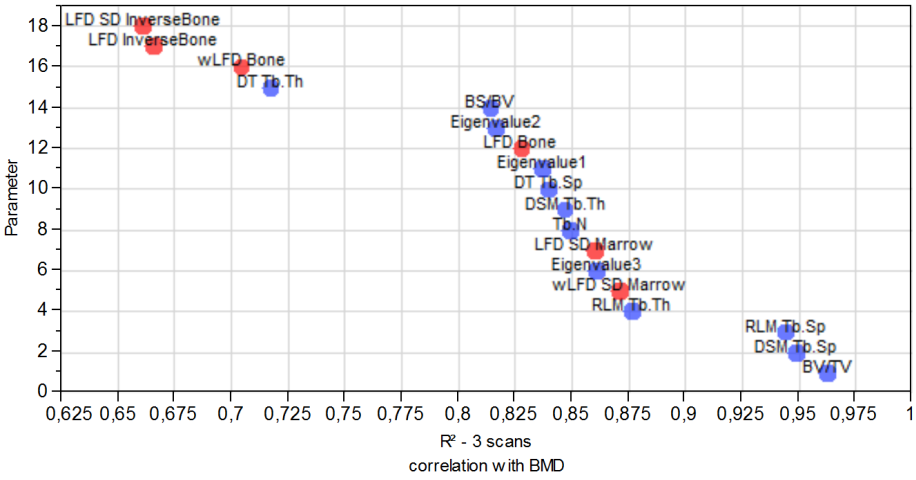

Fig. 5. Correlation of the structure parameters with the BMD with 3 repeated scans without body rings, axes are as in Fig. 4. The $\mathrm{LFD}_{\mathrm{InverseBone}}$ and $\mathrm{wLFD}_{\mathrm{Bone}}$ show the lowest correlation with the BMD, followed by $\mathrm{Tb.Th}_{\mathrm{DT}}$ and BS/BV.

μCT's BV/TV ($R^2 = 0.816$). However, the second eigenvalue and the BS/BV showed similar behavior for these structure parameters, see Fig. 7.

4 Discussion and conclusion

The theoretical information of the LFD distribution is related with the structure model index [10]. The Hölder exponent α describes the fractal dimension of the local underlying structure and is 3, if the voxel is completely surrounded by other bone, 2 if the voxel is part of a plate, 1 if the voxel is part of a rod and 0 if the voxel is isolated. In that sense, the average LFD is in theory a number describing the plate-likeness or rod-likeness of the specimen. Conversely, in applied HRCT imaging the bone is blurred and not thin, therefore higher Hölder exponents are assigned to interior voxels compared to the outer ones. Due to that fact, we measure with $\mathrm{wLFD}_{\mathrm{Bone}}$ partially as well the Tb.Th.

We used in this paper a linear fit to exclude the influence of the BMD from the structure parameters and as well a linear model (ANOVA) to extract the information generated by the certain structure parameters. This yields to the paradoxical result, that e.g. BS/BV and $\mathrm{Tb.Th}_{\mathrm{DSM}}$ show different precisions, although they contain the same information but are reciprocal to each other. Future analyses could resolve this issue by using more advanced methods.

Future analyses could deal with larger sets of in-vivo scans. We have access to a set of 33 HRCT in-situ-scans of osteoporotic T12 vertebrae with known fragility and 3 different treatment histories: not treated subjects, subjects treated with bisphosphonates between 1-5 years, and subjects treated longer than 5 years [6].

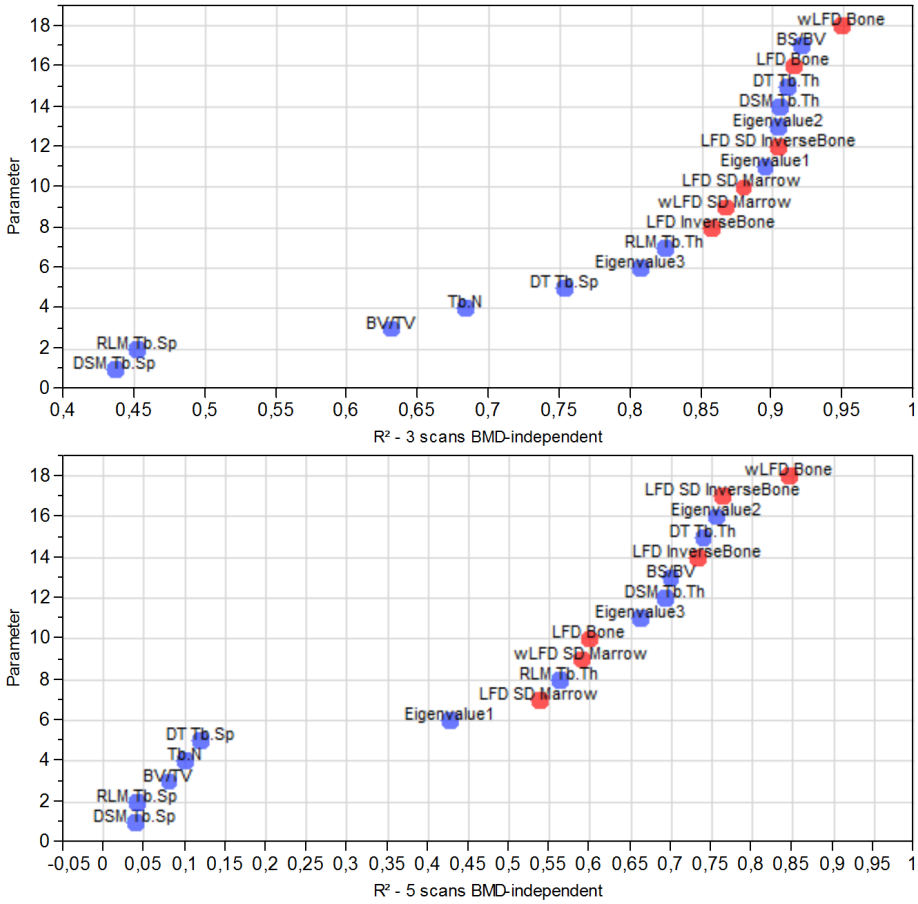

Fig. 6. The BMD-independent precisions explain the information that was not induced by the BMD. For the setting with 3 repeated scans without body rings, the $\text{wLFD}_{\text{Bone}}$ was most precise followed by BS/BV and LFD_{Bone} (top figure). The setting with additional 2 scans with body rings decreased the precisions. The best parameter was however still $\text{wLFD}_{\text{Bone}}$ whereas BS/BV relatively lost precision (bottom figure).

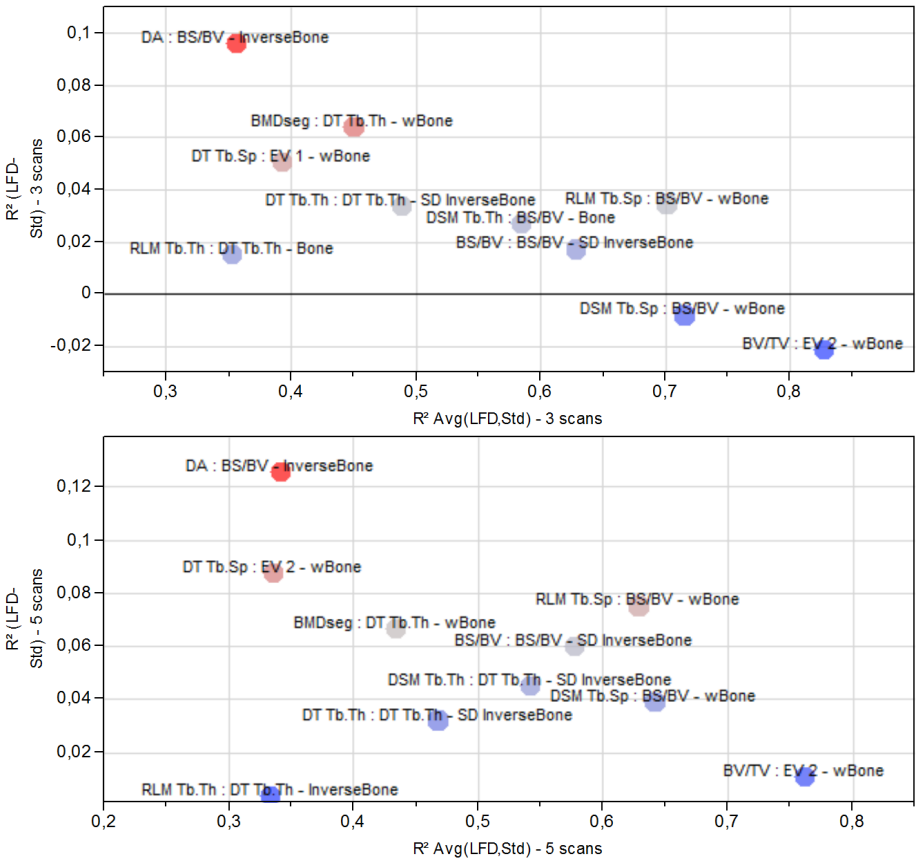

Fig. 7. Each μCT-parameter is approximated with HRCT-standard methods and HRCT-LFD methods. We plot the modulus of the R^2 between μCT- and HRCT-standard methods and the modulus of the R^2 between μCT- and LFD-method. The x-axis contains the average of the modulus of the R^2's and the y-axis contains the difference of the modulus of the R^2's. The diagram depicts the correlation between μCT-parameters and the best HRCT parameters without body rings. The labels show the 3 structure parameters with syntax (in Backus-Naur form): < μCT-parameter>:<HRCT-parameter> − <LFD-parameter>. For the setting with 3 scans $\text{Tb.Sp}_{\text{DSM}}$ and BV/TV were the only parameters which have been better approximated with standard methods than with LFD methods (top figure). The setting with 5 scans shows the robustness of the LFD methods to explain μCT-parameters. Every μCT-parameter could be explained more accurate by the LFD-methods and the difference of the R^2 increased against the setting with 3 scans although the data was disturbed by the 2 additional scans with body rings (bottom figure).

Another available data-set consists of in-vivo scans with 3 visits per subject, tracking the effect of bisphosphonate-treatment.

Also it is promising to extend the binary LFD to gray-scale LFD by using the input-image directly or an adequate gray-scale signal transform, for example the monogenic signal [4]. Extensions to gray-scale were done for the Tb.Sp by using the fuzzy distance transform (see [11] and [1]) or granulometric analyses [14]. There are also methods to achieve a gray-scale local fractal dimension and to derive a multi-fractal spectrum from the LFD-map [15].

The BS/BV shows as well high precision in the ANOVA test and explains many parameters of the μCT. Also the closely related $\mathrm{Tb.Th_{DT}}$ shows good results. This is an unexpected behavior as the HRCT resolution of $188 \times 188 \times 300\mu m^3$ is too coarse for measuring Tb.Th which is expected to be in between $80 - 200\mu m$, but agrees with earlier observations where BS/BV was found to discriminate antiresorptive and osteoanabolic treatment at in-vivo HRCT-resolution [5].

The LFD was the superior approach to translate existing structure parameters from μCT to clinical HRCT. Nevertheless, the gap between μCT and HRCT measurements likely indicates the necessity of using more sophisticated analytical methods for extrapolating the information from HRCT to μCT-scans. In particular, $\mathrm{wLFD_{Bone}}$ appeared precise and robust against noise, and was the best new qualitative structure parameter. We propose that $\mathrm{wLFD_{Bone}}$ can be used as a high precision qualitative structure parameter. It provides additional information to the standard structure parameters and is minimum biased by the BMD.

Acknowledgments. This work benefited from the use of the Insight Segmentation and Registration Toolkit (ITK), available at www.itk.org and the GUI-library Qt, accessible at qt-project.org. The work was founded by the Molecular Imaging North Competence Center (MOIN CC), Biomechanically Founded Individualized Osteoporosis Assessment and Treatment (BioAsset), Accelerated Image Processing and Visualization: Applications in Environmental Sciences and Healthcare (MICROSOFT-LACCIR) and Consejo Nacional de Investigaciones Científicas y Técnicas (CONICET). F. Thomsen acknowledges the assistance of V.A. Guinder in improving the manuscript and gratefully thanks the reviewers and the editor.

References

1. Darabi, A., Chandelier, F., Baroud, G.: Thickness analysis and reconstruction of trabecular bone and bone substitute microstructure based on fuzzy distance map using both ridge and thinning skeletonization. Canadian Journal of Electrical and Computer Engineering 34, 57–62 (2009)
2. Dempster, D.W.: The impact of bone turnover and bone-active agents on bone quality: focus on the hip. Osteoporosis international 13, 349–352 (2002)
3. Dougherty, G.: Medical Image Processing - Techiques and Applications. Springer, New York (2011)

4. Felsberg, M., Sommer, G.: The monogenic signal. IEEE Transactions on Signal Processing 49, 3136–3144 (2001)
5. Glüer, C.-C., Marin, F., Ringe, J.D., Hawkins, F., Möricke, R., Papaioannu, N., Farahmand, P., Minisola, S., Martínez, G., Nolla, J.M.: Comparative effects of teriparatide and risedronate in glucocorticoid-induced osteoporosis in men: 18-month results of the EuroGIOPs trial. J Bone Miner Res. 28, 1355–1368 (2013)
6. Glüer, C.-C., Krause, M., Museyko, O., Wulff, B., Campbell, G., Damm, T., Daugschies, M., Huber, G., Lu, Y., Peña, J., Waldhausen, S., Bastgen, J., Rohde, K., Steinebach, I., Thomsen, F., Amling, M., Barkmann, R.: New horizons for the in vivo assessment of major aspects of bone quality: microstructure and material properties assessed by Quantitative Computed Tomography and Quantitative Ultrasound methods developed by the BioAsset consortium. (to appear)
7. Graeff, C., Timm, W., Nickelsen, T.N., Farrerons, J., Marin, F., Barker, C., Glüer, C.-C.: Monitoring Teriparatide-Associated Changes in Vertebral Microstructure by High-Resolution CT In Vivo: Results From the EUROFORS Study. J Bone Miner Res. 22, 1426–1433 (2007)
8. Graeff, C.: Bone Strength Surrogate Markers. PhD thesis, Technische Universität Hamburg-Harburg (2010)
9. Hildebrand, T., Rüegsegger, P.: A new method for the model-independent assessment of thickness in three-dimensional images. Journal of Microscopy 185, 67–75 (1997)
10. Hildebrand, T., Rüegsegger, P.: Quantification of bone microarchitecture with the structure model index. Comput Methods Biomech Biomed Engin. 1, 15–23 (1997)
11. Krebs, A., Graeff, C., Frieling, I., Kurz, B., Timm, W., Engelke, K., Glüer, C.-C.: High resolution computed tomography of the vertebrae yields accurate information on trabecular distances if processed by 3D fuzzy segmentation approaches. Bone 44, 145–152 (2009)
12. Lopes, R., Betrouni, N.: Fractal and multifractal analysis: A review. Medical Image Analysis 13, 634–649 (2009)
13. Majumdar, S., Kothari, M., Augat, P., Newitt, D.C., Link, T.M., Lin, J.C., Lang, T., Lu, Y., Genant, H.K.: High-resolution magnetic resonance imaging: three-dimensional trabecular bone architecture and biomechanical properties. Bone 22, 445–454 (1998)
14. Moreno, R., Borga, M., Smedby, Ö.: Estimation of trabecular thickness in gray-scale images through granulometric analysis. Proceedings of SPIE, San Diego (2009)
15. Nilsson, E.: Multifractal-based image analysis with applications in medical imaging. Masters thesis Umea University (2007)
16. Novianto, S., Suzuki, Y., Maeda, J.: Near optimum estimation of local fractal dimension for image segmentation. Pattern Recognition Letters 24, 365–374 (2003)
17. Parfitt, A.M., Drezner, M.K., Glorieux, F.H., Kanis, J.A., Malluche, H., Meunier, P.J., Ott, S.M., Recker, R.R.: Bone histomorphometry: standardization of nomenclature, symbols, and units: report of the ASBMR Histomorphometry Nomenclature Committee. J Bone Miner Res. 2, 595–610 (1987)
18. Simmons, C.A., Hipp, J.A.: Method-Based Differences in the Automated Analysis of the Three-Dimensional Morphology of Trabecular Bone. Journal of Bone and Mineral Research 12, 942–947 (1997)
19. Skyscan: Structural parameters measured by Skyscan CT-analyzer software. Manual, Skyscan (2009)